SCHOOL OF PHYSICS AND ASTRONOMY

YEAR 3 FINAL PROJECT REPORT

SESSION 2019-2020

Name:	**Ryan Alexander**
Student Number:	**C1769257**
Degree Programme:	**Physics and Astronomy BSc**
Project Title:	**Can We Make Waveguides with a Negative Refractive Index? Finding and Characterising Modes in a Negative Refractive Index Waveguide with the Finite-Difference Time-Domain Method**
Supervisor:	**Dr Daryl Beggs**
Assessor	**Dr Amy Morreau**

Declaration:

I have read and understand Appendix 2 in the Student Handbook: "Some advice on the avoidance of plagiarism".

I hereby declare that the attached report is exclusively my own work, that no part of the work has previously been submitted for assessment (although do note that material in "Interim Report" may be re-used in the final "Project Report" as it is considered part of the same assessment), and that I have not knowingly allowed it to be copied by another person.

Can We Make Waveguides with a Negative Refractive Index? Finding and Characterising Modes in a Negative Refractive Index Waveguide with the Finite-Difference Time-Domain Method

Ryan Alexander, C1769257

May 2020

Abstract

Two modes were found and studied in a negative refractive index waveguide, with the finite-difference time-domain method, confirming that a negative index waveguide can propagate guided modes. It was found that these modes had turning points in their dispersion relations, implying an inversion of group velocity within the mode, as well as double degeneracy at certain frequencies within the mode. Double degeneracy was found at frequencies between 370 and 372THz, and 360 and 362THz, for each mode respectively, with turning points being found at the peak of those frequency ranges. The group velocity of light in the modes was found to be between 0 and 0.2 (normalised, c=1 units) for the majority of wavenumbers, before passing through 0 and approaching -1 at the highest wavenumbers. Both of these findings are consistent with previous studies of modes in negative refractive index waveguides. It was also found that the transmission in negative index materials obeys the Beer-Lambert law, using the finite-difference time-domain method.

Contents

1 Introduction

1.1 Aims - Finding and Characterising Modes in a Negative Refractive Index

This project aimed to determine the characteristics of a negative refractive index waveguide through numerical simulations using the program, Lumerical FDTD. The project aimed to determine the suitability of the finite-difference time-domain method for simulating negative index materials. The project also aimed to create a negative index material and characterise the absorptivity of the material and the factors that affect it. Finally, the project aimed to find modes in a negative refractive index waveguide and find novel properties found in previous studies [1][2][3], using the finite-difference time-domain method.

1.2 Literature Review and Basic Theory

1.2.1 Negative Refractive Index

The permittivity and permeability of a material quantifies the ability of a material to become polarized and store energy in the electric and magnetic field respectively. According to Maxwell's equations:

$$n = \sqrt{\epsilon\mu} \tag{1}$$

where n is the index of refraction, ε is the permittivity and μ is the permeability of the material.

Theoretically, light in a material with negative permittivity and permeability would have many novel and potentially useful properties. For example Maxwell's equations imply such a material would cause light to refract to the opposite side of the normal as seen in all positive index of refraction materials (shown in figure 1). It can also be seen from Maxwell's equations that light in such a material would have a phase vector opposite to the wave vector resulting in a reversing of the Doppler effect and other phenomena [4].

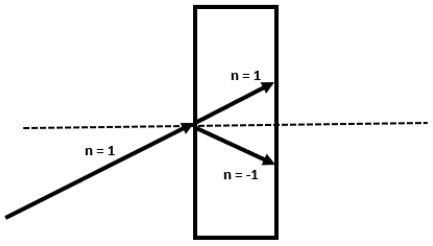

Figure 1: An illustration of the inversion of Snell's law. If the refractive index is negative the beam refracts to the same side of the normal as the incident beam.

To account for the light refracting on the same side of the normal as the incident light, and to keep the refractive index consistent with Snell's law, Veselago proposed a correction to the refractive index equation in 1968:

$$n = \pm\sqrt{\epsilon\mu} \tag{2}$$

where the positive value is taken if ε and μ are both positive and the negative if ε and μ are both negative [4]. It can therefore be said that materials with a negative ε and μ are negative index of refraction materials and that they are possible in theory.

A potential use for a negative refractive index material is in the creation of a perfect lens. The angular resolution of a lens is limited by the diffraction limit (or Rayleigh Criterion) for that lens, at which two separate light sources become indistinguishable due to the overlap of their Airy disks. The minimum angular resolution for a lens is given by:

$$\sin(\theta_R) = 1.22\frac{\lambda}{2r} \tag{3}$$

where ϑ_R is the angular resolution, λ is the wavelength of light being observed and r is the radius of the lens [5]. In 2000, J. B. Pendry showed that a slab of negative refractive index material could act as a perfect lens (a lens with a resolution surpassing the diffraction limit) due to light refracting to the same side of the normal [6].

There are no known naturally occurring materials with a negative refractive index; however, they can be created in the form of metamaterials (man-made materials that exhibit properties not found in natural materials). In 1999 it was demonstrated that a periodic array of conducting resonators could be used to create a one dimensional metamaterial with negative permittivity and permeability at microwave wavelengths [7]. A year later the negative index of refraction metamaterial was extended to two dimensions [8]. Finally, one year later there was direct experimental confirmation that the metamaterial had a negative index of refraction after incident light was refracted to the same side of the normal, confirming Veselago's prediction [9].

1.2.2 Waveguides

A waveguide is a structure that transmits light, by use of guided modes, along its length. By restricting the transmission of light to one dimension, the inverse square law governing the power of transmitted light is negated. Thus the only factor restricting the efficiency of the transmission of the waves is the absorptivity of the medium in the waveguide. The most widely known example is that of optical fibres. Due to constructive and destructive interference there are certain frequencies at which a waveguide will function, depending on its structure. These frequencies excite modes in the waveguide [10]. A potentially useful but

relatively unexplored application of negative index materials is in waveguides. 2002 [2], 2003 [1] and 2018 [3] papers found that the modes in negative index waveguides exhibited unusual characteristics such as turning points in their dispersion relations [3], no fundamental modes and novel mode profiles (shown in figure 2) amongst others [1]. It has even been suggested that negative refractive index waveguides could be used to slow, stop or even reverse the group velocity of light which could have interesting applications in optical technologies [2].

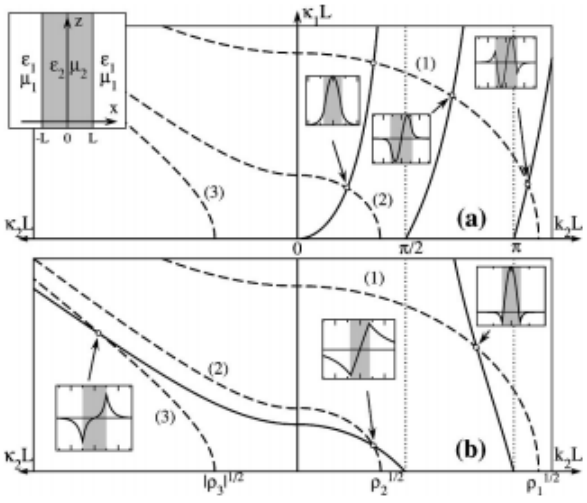

Figure 2: Graphs of the first three solutions to the dispersion relations (the first three guided modes) in a positive (a) and negative (b) refractive index waveguide. The modes are plotted at the solutions. Figure from [1].

1.3 Relevant Techniques and Theory

1.3.1 The Finite-Difference Time-Domain Method

Finite difference methods approximate differential equations by using a truncation of the Taylor series:

$$f(x_0 + h) = f(x_0) + \frac{f'(x_0)}{1!}h + R_1(x) \tag{4}$$

which, assuming $R_1(x)$ is sufficiently small, can be rearranged to give:

$$f'(x) \approx \frac{f(x+h) - f(x)}{h} \tag{5}$$

The program Lumerical FDTD ("Lumerical" hereafter) is designed for simulating how light will propagate through nanophotonic devices. Throughout this project, Lumerical has been used to investigate the photonic properties of negative refractive index materials. Lumerical uses the finite-difference time-domain method to solve Maxwell's equations numerically. In two dimensional simulations it is assumed that the structure of the simulation is infinite and uniform in the Z-direction. The magnetic field (H) and electric field (E) vectors can then be grouped into the transverse magnetic (H_x, H_y, E_z) and transverse electric (E_x, E_y, H_z) polarisations, each having their own independent set of Maxwell's curl equations giving H and E in two dimensions respectively [11]. Applying equation 5 to these equations allows for the magnetic and electric fields to be calculated numerically by progressing through time steps. For example, an equation for the y-component of the magnetic field can be given by equation 6:

$$H_y(t + \Delta t) = \frac{\Delta t}{\sqrt{\epsilon_0 \mu_0}} \frac{\partial E_z(t)}{\partial x} + H_y(t) \tag{6}$$

Allowing for the y-component of the magnetic field to be evolved in time, based on the previous E and H fields [11]. The program calculates these electromagnetic field values across time at a field of points on a user defined grid.

In practice, numerical methods can not be applied to infinitely large electromagnetic fields. Therefore it is necessary to truncate the region being simulated with boundary conditions. In this project the two boundary conditions used are PML (perfectly matched layer) and periodic boundary conditions. PML boundaries are artificial layers of material which, in the perfect case, absorb all light incident on them without reflecting. This allows for a region in space to be simulated as if it was surrounded by infinite empty space, as there is no difference to the electromagnetic field in the simulation region between outgoing light being absorbed by the PML and outgoing light propagating infinitely into empty space. Periodic boundary conditions on the other hand allow for one region of an infinitely repeating (periodic) system to be simulated. One periodic boundary absorbs any incident light and the opposite boundary emits identical light. For example an infinite square lattice of light sources can be reduced to

a unit cell (a rectangular region of space) containing a source. If light leaves this unit cell it re-enters the cell at the opposite boundary resulting in identical electromagnetic fields to the case in which all sources were being simulated and the adjacent source had emitted the light.

The FDTD method will theoretically converge with the exact analytical solution as the time steps used in the approximation are reduced in size [12]. As Lumerical does not use a continuous field, but rather points on a mesh, the FDTD approximation will also theoretically converge with the analytical solution as the distance between mesh points is decreased.

1.3.2 Lumerical's Magnetic Electric Lorentz Material

A magnetic and electric Lorentz material is included in Lumerical which uses the following equations to determine permittivity and permeability [13]:

$$\epsilon(\omega) = 1 + \chi_e + \frac{\Delta\epsilon\omega_e^2}{\omega_e^2 - 2i\delta_e\omega - \omega^2} \tag{7}$$

$$\mu(\omega) = 1 + \chi_m + \frac{\Delta\mu\omega_m^2}{\omega_m^2 - 2i\delta_m\omega - \omega^2} \tag{8}$$

where χ is the susceptibility, ω is the angular frequency and δ is the loss angle which determines the imaginary part of the permittivity and permeability and therefore the loss of the material. It is possible for the permittivity and permeability to be simultaneously negative at specific frequencies, depending on the values input into equations 10 and 11. If the permittivity and permeability equations are set up to be equal the refractive index will be equal to both the permittivity and permeability and a graph of the real parts of either can be used to determine the real part of refractive index at specific wavelengths.

1.3.3 The Beer-Lambert Law

The rate at which light is attenuated in a material is called the absorptivity. It is related to the light transmitted and the distance light travels though a material by the Beer-Lambert law [14]:

$$\ln(T) = -al \tag{9}$$

where a is the absorptivity of the material, l is the length of material that the light passes through and T is the ratio of light transmitted across the material. According to equation 9, a graph of ln(T) against length will have a gradient of the absorptivity of the material used.

1.3.4 Modes in a Waveguide and Their Properties

When exciting modes in a given structure with a point source, the modes which are excited are sensitive to the position of the source. When placing a source

in a waveguide, the overlap of the wavefunction generated by that source with the possible modes in the waveguide determines the excitation of each mode. To excite a mode with a point source, care would have to be taken not to place the source at one of the desired modes' nodes as this would result in the wavefunctions of the mode and source being orthogonal and the source would not excite the mode. For example, a point source placed in the centre of the waveguide shown in figure 3 could excite odd numbered modes 1, 3 and 5 but not the even numbered modes with nodes in the centre of the waveguide.

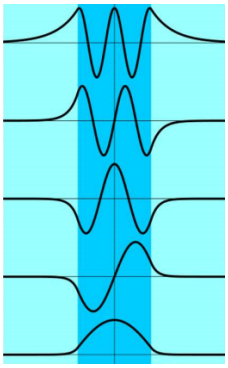

Figure 3: Cross sections of the first five modes of the same polarisation in a one-dimensional dielectric waveguide. Figure from private communication with supervisor.

Figure 3 shows modes of one polarisation. Modes can have one of two polarisations, named "transverse electric" and "transverse magnetic" depending on which plane their electric and magnetic field lines are confined to. The polarisation of the modes excited in a waveguide can be controlled by the polarisation of the light source.

A useful property of guided modes in a waveguide is their effective refractive index (n_{eff}). The effective refractive index is the ratio of the speed of light in a vacuum to the speed of a mode along the length of a waveguide. For example, if the waveguide is designed to guide light along the x-direction then the effective refractive index is given by:

$$n_{eff} = \frac{c}{v_x} \tag{10}$$

where c is the speed of light and v_x is the x-component of the phase velocity of the light as shown in figure 4 below. Figure 4 and figure 3 show how some of the electromagnetic field leaks into the material surrounding the waveguide. This is known as the evanescent wave and causes the refractive index outside of the surrounding material to contribute to the effective refractive index of the modes.

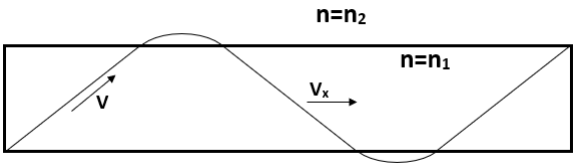

Figure 4: An illustration of the path of a wavefront in a guided mode in a dielectric waveguide. The waveguide is positioned along the x-direction. The phase velocity and the x-component of the phase velocity (related to the effective refractive index) have been labelled.

The effective refractive index can be used to find the x-component of the angular wavenumber (k_x) using definitions $v = \lambda f$ (v = phase velocity), $k = \frac{2\pi}{\lambda}$ [15] and equation 10:

$$k_x = \frac{2\pi n_{eff} f}{c} \tag{11}$$

If data is obtained for both the frequency and wavenumber of light in a material a dispersion relation can be plotted. This is especially useful when the possible frequencies and wavenumbers for a specific mode are plotted. When this is done the graph reveals how the frequency of light affects the wavenumber and thus effective refractive index and group velocity of the mode. This is due to the fact that, in order to constructively interfere and form a mode, the wavefront in figure 4 must be out of phase with itself by π radians each time the beam reaches an edge of the waveguide. To satisfy this condition there is a discrete angle at which the wavefront propagates at for each mode, which is a function of the frequency of the light and has the following effect on the wavenumber: $k_x = k\cos\theta$. The group velocity can then be found with equation 12, which is the gradient of a dispersion relation showing angular frequency against wavenumber [16].

$$\frac{\partial\omega}{\partial k} = v_g \tag{12}$$

1.3.5 Dispersion Relation Lines in Periodic Simulations

In a periodic structure, dispersion relation graphs are periodic and split into Brillouin zones. Periodic boundary conditions, spaced width "a" apart, can be used to simulate a section of waveguide and have the simulation behave as a boundless simulation of an infinite, repeating array of the simulated section of waveguide. This also applies to sources meaning if there is a source in the periodic simulation, the simulation will produce results as if there are infinitely many, periodically spaced by "a", sources in the waveguide[1]. Taking a snapshot of a single Brillouin zone leads to dispersion relations which appear "reflected"

[1]The simulation is not actually creating infinite, repeating sections of waveguide and sources (although the results are identical). It is simply allowing light that exits one boundary of the simulation to re-enter at the opposite boundary as if it had come from an identical simulation adjacent to the original area as explained in section 1.3.1.

or "folded" at the Brillouin zone boundaries as shown in figure 5a. They are not actually folded, they can be thought of as the dispersion lines from other Brillouin zones created by the periodic boundary conditions. These can be "unfolded" to find the true dispersion relation by reflecting the dispersion lines at the Brillouin zone boundaries, as shown in 5b.

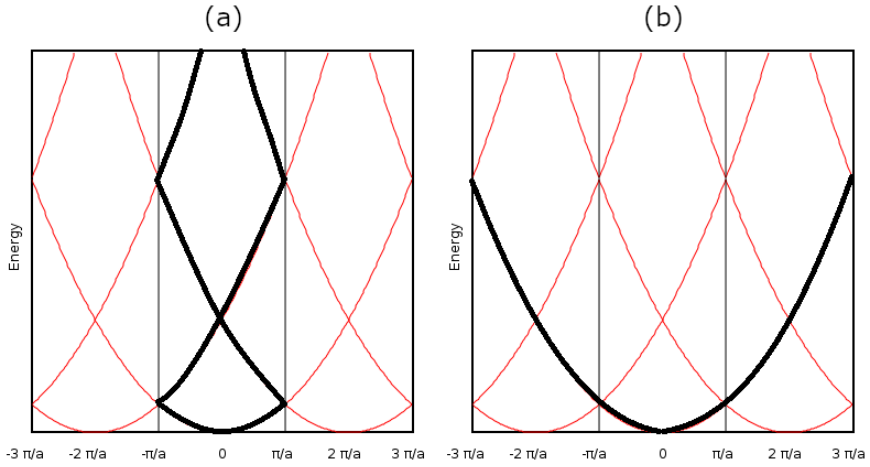

Figure 5: Figure a shows how taking a snapshot of the dispersion relation within one Brillouin zone leads to a "folding" effect which can be thought of as dispersion lines from other Brillouin zones entering the central, simulated zone. Figure b shows how reflecting the dispersion lines at the Brillouin zone boundaries can give the true dispersion relation that would be found with a larger simulation width. Figure adapted from [17]

2 Creating and Testing a Negative Index Material in Lumerical FDTD

2.1 Creating the Material

A material with a negative index of refraction was created in Lumerical, using the magnetic electric Lorentz material which defines a material with permittivity and permeability defined by equations 7 and 8. The following values were used in the material: susceptibility χ_e and χ_m equal to 0, $\Delta\varepsilon$ and $\Delta\mu$ equal to 1, ω_e and ω_m equal to 2×10^{15} and loss angle δ_e and δ_m equal to 1×10^{13}. This gave a refractive index of -1 at approximately $\lambda = 769.1$nm using equations 7 and 8. The inversion of Snell's law was tested by creating a slab of negative index material and shining a beam of light (with wavelengths including 769.1nm) at an angle of 45 degrees onto its surface. At $\lambda = 769.1$nm the beam refracted to the same side of the normal, as predicted by Veselago [4], confirming that the material had a negative index of refraction at that wavelength.

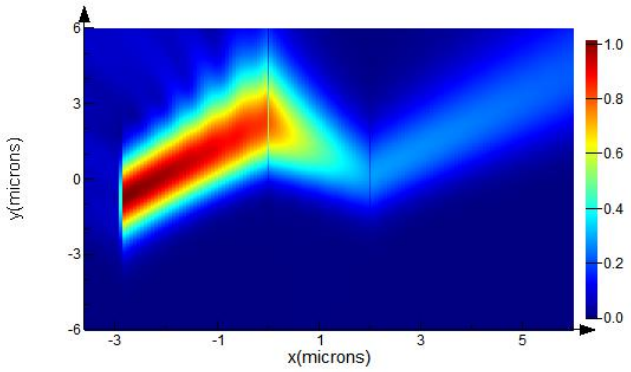

Figure 6: A heat-map of the electric field magnitude, at $\lambda = 769.1$nm, of a beam of light incident on a slab of negative refractive index material between $x = 0$ and $x = 2$ microns. The incident wave can be seen to refract to the same side of the normal (as described in section 1.2.1) at the material's boundaries confirming that Snell's law is inverted.

2.2 Convergence Testing

To increase confidence that the FDTD method was approximating accurately for negative index materials, "convergence tests" were run to ensure that various values found using the FDTD method were converging on a true value as the accuracy of the method was increased. Where possible, these values were checked against analytical solutions.

It can be shown that at normal incidence, the reflectance of a boundary given

by the Fresnel equation simplifies to:

$$R = \left(\frac{n_1 - n_2}{n_1 + n_2}\right)^2 \tag{13}$$

where R is the proportion of light that is reflected [18]. Using equation 12, the proportion of light from a plane wave source that is transmitted across a boundary between two media can be found analytically. To test if values for reflection and transmission found by the FDTD method converge on discrete solutions a plane wave source was positioned normally incident to a vacuum-dielectric boundary in Lumerical. The dielectric was set to have refractive index 2 and no loss so that any incomplete transmission of light would be due to reflection at the boundary. Periodic boundary conditions were used at the y-boundaries of the simulation and PML x-boundaries were used. The amount of light transmitted through the boundary was measured for a range of different mesh sizes and compared to the analytical solution found with equation 13 as shown in figure 7. It was found that a mesh size of 10nm gave an error in transmission of 0.0007 or 0.08% of the analytical solution. It is possible for a numerical solution to happen to be accurate under specific conditions. For example the transmission calculated with a mesh size of 0.07μm was by chance within 1% of the analytical solution. The points either side at 0.06μm and 0.08μm are less accurate, implying that the point at 0.07μm is accurate by chance and the point would not maintain its accuracy under different simulation conditions (e.g. changing refractive index slightly). In contrast, the points either side of the 10nm value (5nm and 15nm) were also within 0.1% of the analytical solution, increasing confidence that the point was not accurate by chance.

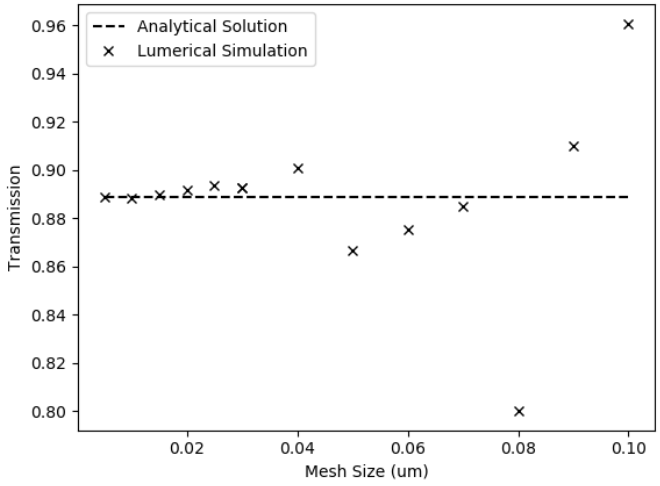

Figure 7: A graph of transmission across an n=1 to n=2 boundary against mesh size, including an analytical solution. It can be seen that as mesh size is reduced, the numerical solutions converge with the analytical solution.

The convergence of the attenuation of a slab of negative index material was also tested. A plane wave source positioned normally incident to a slab of negative index material was created. Periodic "y" and PML "x" boundaries were used. The transmission to the other side of the material was measured for varying mesh sizes. Although no analytical solution was calculated, the data is still useful as the transmission is seen to converge on a value as the mesh size is decreased. This is shown in figure 8. The values of transmission at the final 5 mesh sizes (8-15nm) were within 1% of the value found at the smallest mesh size.

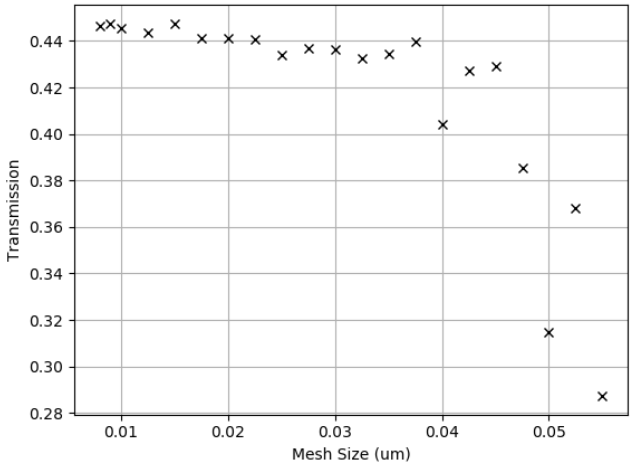

Figure 8: Transmission across a slab of negative index material against mesh size used. Once again, it can be seen that as mesh size is reduced the calculated value of transmission converges to a discrete, "true" value.

Based on these convergence tests it was decided that a mesh size of 10nm in the FDTD method gave sufficiently accurate results for transmission, reflection and attenuation.

3 Investigating Loss in the Negative Index Material

3.1 Confirming the Beer-Lambert Law for Negative Index Materials

3.1.1 Methodology

In figure 6 it can be seen that the negative index material is attenuating some of the light. One of the most fundamental laws of optics is the Beer-Lambert law described in section 1.3.3 with equation 9. An experiment was designed to confirm that the negative index material obeyed the Beer-Lambert law. Lumerical simulations were run with plane waves passing normally through a slab of the negative index material, identical to the one created in section 2. A mesh size of 10nm was used. All transmission data was taken at $\lambda = 769.1$nm, where $n = -1$. Due to the magnitude of the refractive indices being the same on either side of the boundary, no reflection was expected in the simulation.

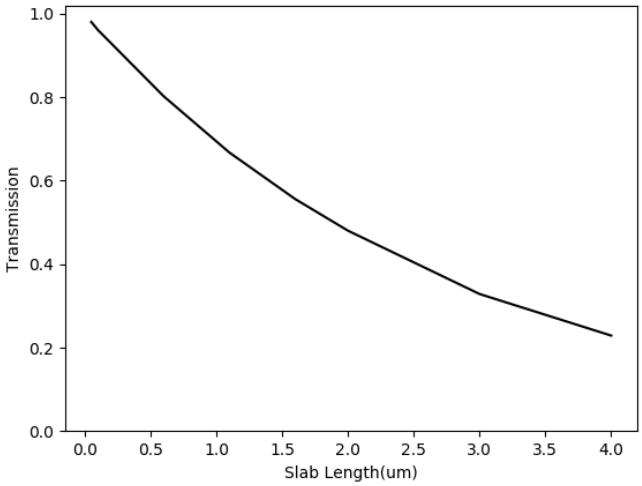

Figure 9: A graph of transmission through a slab of negative index material against slab length. As expected, the data takes the form of an exponential decay in agreement with the Beer-Lambert law.

Fitting a line to the natural log of transmission against slab length allows for the absorptivity to be given by the gradient of the line as explained in section 1.3.3.

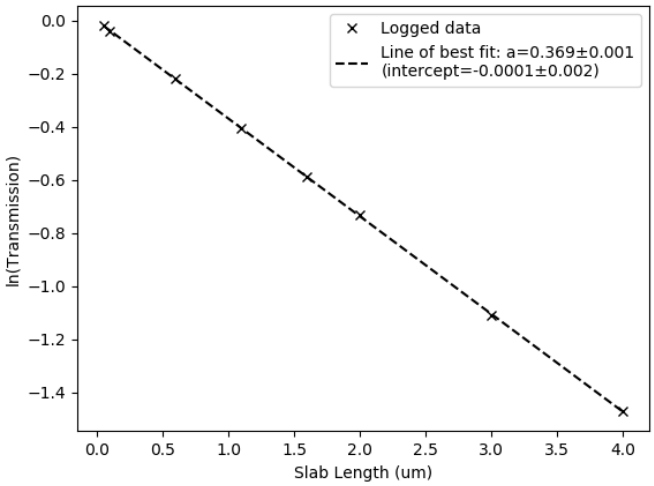

Figure 10: A graph of the natural log of transmission through a slab of negative index material against slab length. As expected the data forms a straight line. The gradient of the line of best fit is used to give the absorptivity of the material.

3.1.2 Results and Discussion of Absorptivity in Negative Index Materials

Figure 9 shows that the negative index material assumed the exponential decay of transmission against slab length described by the Beer-Lambert law. The straight line formed in figure 9 confirms that the absorptivity is governed by an equation of the form $ln(T) = -al$, confirming that the material is governed by the Beer-Lambert law. In this case the absorptivity, "a" of the material was found to be $(0.369 \pm 0.001)\mu m^{-1}$. The line of best fit was expected to pass through the origin (as a widthless slab is unable to attenuate light). In agreement, its y-intercept had an error range that encompassed the origin. While this was performed for a material with permittivity and permeability defined by equations 7 and 8, these equations simply provide complex values for permittivity and permeability, hence it is assumed that the Beer-Lambert law would would hold true for any negative index material with complex permittivity and permeability, regardless of how these values are generated.

3.2 Investigating Loss Angle

Next, the relationship between the loss angles, δ, in equations 7 and 8 and the absorptivity of a slab of the negative index material was investigated. A similar setup with a plane wave incident on a slab of width 1μm was used. δ_e and δ_m were kept equal and were varied incrementally from 1×10^{13} to 5×10^{13}. The transmission across the slab was recorded for each loss angle. Inputting values into equations 7 and 8, it was found that respective δ values have very little effect on the real part of the permittivity and permeability. At $\lambda = 769.1$nm (n=1), increasing the loss angle by a factor of 5 resulted in a 0.029 decrease in the refractive index (a 3% decrease). Inputting this change in refractive index into the Fresnel equation (equation 13) showed that the change in refractive index would cause the transmitted light to decrease by 0.02%. It was therefore concluded that the transmission data could be sampled at the same 769.1nm wavelength for loss angles between 1×10^{13} and 5×10^{13} and any significant change in the ratio of transmitted light was due to a change in the absorptivity of the material, not reflection at the vacuum-slab boundaries. As detailed in the previous section, data was collected for transmission across slab widths between 0.1 and 3.6 μm for each loss angle. Again, a mesh accuracy of 10nm was used. The natural log of this data was taken to calculate the absorptivity at each loss angle. Figure 11 shows absorptivity against loss angle and suggests that absorptivity is directly proportional to loss angle. Furthermore, assuming a linear relationship, a loss angle to absorptivity coefficient of $(0.371 \pm 0.002) \times 10^{13}\mu m^{-1}$ was found. This is in agreement with the absorptivity of $(0.369 \pm 0.001)\mu m^{-1}$ for loss angle 10^{13} calculated in section 3.1.

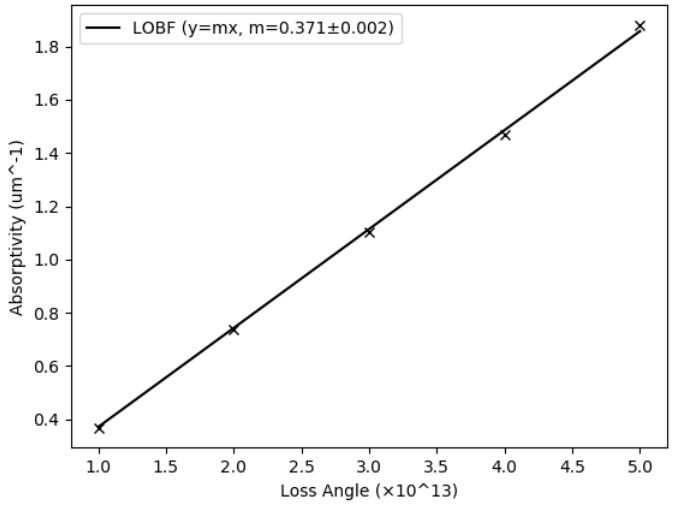

Figure 11: A graph of absorptivity against loss angle δ, ($\delta = \delta_e = \delta_m$). A line of best fit shows a loss angle to absorptivity conversion coefficient of 0.371 ± 0.002.

3.3 How Realistic is this Material?

As explained in section 1.2.1, meta-materials can be made with simultaneously negative permittivity and permeability. Equations 7 and 8, used in the creation of the negative refractive index material, provide both dispersion and loss which is observed in the meta-materials which have been created [7][8][9], providing some realism to the material. Furthermore, as in real materials, the Beer-Lambert law has been shown to hold true in the negative index material. Finally, the loss angle has been shown to linearly affect the absorptivity of the material, allowing for the material to be fine-tuned to match real life materials if needed.

4 Looking for and Characterising Modes in a Negative Index Waveguide

4.1 Developing a Method for Finding Modes

Lumerical provides a "mode expansion monitor" [19], hereafter "mode monitor", which can be used to find modes in a positive index waveguide. When simulating a two-dimensional waveguide, the mode monitor can be placed on an arbitrary one-dimensional cross section of the waveguide and the surrounding material, sampling the refractive indices of both. The mode monitor then establishes boundary conditions for the E and H fields in the waveguide and finds a set of modes which satisfy these boundary conditions. While this proves to be a valid method for finding and characterising modes in positive waveguides, for reasons beyond the scope of this project, the mode monitor is unable to establish modes for a negative refractive index waveguide. It is therefore necessary to develop a new method for finding modes, which can be tested against this mode monitor method on a positive index waveguide, before being applied to a negative index waveguide.

First, a 2D waveguide with width 0.5μm and a dispersionless refractive index of 1.5 was created, designed to create modes travelling along the x-axis. The "y-boundaries" were placed far from the waveguide to ensure minimal absorption of light from modes travelling down the length of the waveguide. The "y-boundaries" were set to PML to absorb any outgoing light. The simulation region was adjusted so that a 0.5μm wide cross section of the waveguide and surrounding vacuum were being simulated. This simulation width will hereafter be referred to as "a" in equations and figures. The "x-boundaries" were set to periodic, resulting in the simulation being identical to a small simulation of an infinitely repeating uniform section of waveguide of width $a = 0.5$μm. As explained in section 1.3.4, when attempting to detect a given mode, care must be taken not to position sources and detectors on the nodes of the mode. An array of 10 randomly positioned dipole sources, or a "dipole cloud", was placed across the waveguide and surrounding vacuum to greatly decrease the number of possible modes that would have sources exclusively placed at their nodes. The orientation of the sources were kept identical and such that only the transverse electric modes (electric field lines confined to the y-z plane) would be excited. For the same reason, an array of 10 randomly positioned time monitors were placed across the waveguide and surrounding vacuum. The simulation region is shown in figure 12.

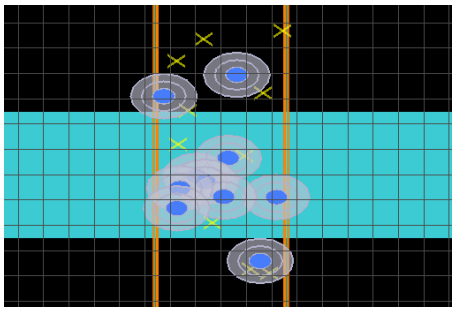

Figure 12: A screenshot showing the positive index waveguide simulation created in Lumerical. The blue rectangle represents the waveguide. The orange lines represent the periodic boundary conditions set up for the "x-boundaries". The circular objects represent the dipole sources and the yellow crosses represent the time monitors. All else is an empty vacuum.

Each time monitor records the electric and magnetic field at their respective positions across time, resulting in amplitude-time data in which non-resonant frequencies decay and resonant frequencies associated with modes persist. Each time-monitor then Fourier transforms their data and adds their Fourier transformed data to a total sum. This results in Fourier amplitude against frequency data shown in figure 13a, in which peaks correspond to resonant frequencies. The periodic boundary conditions can be adjusted to support modes with different x-components of wavenumber (k_x). If the time-monitor method is repeated for a range of different k_x values a dispersion relation graph can be plotted. This method was applied using three different values of k_x and the raw Fourier transformed data as well as the dispersion relation are shown in figure 13b.

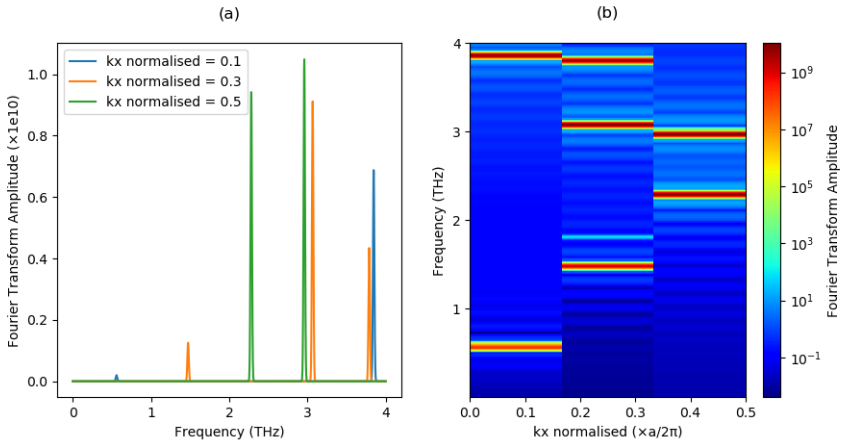

Figure 13: Two graphs showing the Fourier transformed amplitude-time data in (a) and a dispersion relation in (b).

The resolution of this dispersion relation can be improved in two ways. Firstly, the resolution in the x-direction can be improved by increasing the number of k_x values the simulation is run for, simply giving more points in the dispersion relation graph. Secondly, the resolution in the y-direction can be improved by increasing the runtime of the simulation. This allows for the time monitors to detect more peaks related to the resonant frequencies of the waveguide, thus giving more peaks to be used in the Fourier transforms, increasing the resolution of the peaks found by the Fourier transform (shown in figure 13(a)) and therefore reducing the width of the bands plotted in the dispersion relation (shown in figure 13(b)). In figure 14, the number of wavenumbers used was increased to 10 and two FDTD simulations were performed with different runtimes to display the increased resolution in the y-direction.

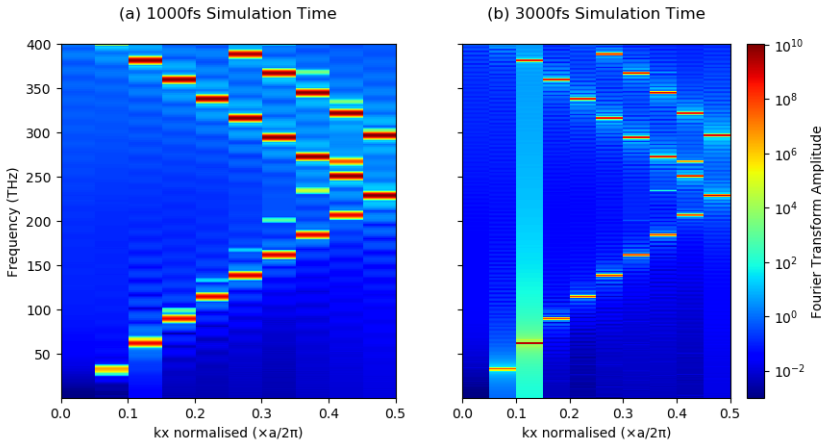

Figure 14: Two dispersion relations showing the increased resolution obtained by increasing the runtime of the FDTD simulation. Figure (a) was produced with a 1000fs runtime and figure (b) was produced with a 3000fs runtime. The first mode is very clear in the above figure and a second mode can also be seen above the first.

Figure 14 shows that increasing the runtime can result in increased accuracy in the y-direction. The increased resolution in the x-axis caused by increasing the number of wavenumber values the simulation was run for can also be seen in figure 14 when compared to figure 13(b). Unfortunately, it also shows an artefact in the form of a vertical line between normalised wavenumbers 0.1 and 0.15. The reason for this is currently unknown and outside of the scope of this project. The maxima relating to the peaks in the Fourier transform are still visible along the wavenumber affected by the artefact. The "folding" of bands explained in section 1.3.5 can also be seen in figure 14.

4.2 Testing the Time Monitor Method

A convergence test was designed for the time monitor method to ensure that the frequency values found by this method were converging on a true value as the accuracy of the FDTD method was increased. The simulation was run with the same 0.5μm waveguide and 0.5μm simulation region. A single normalised x-component of wavenumber was chosen, $k_x = 0.5$. The simulation was run for a range of different mesh sizes (smaller mesh sizes expected to lead to a more accurate simulation) and the maximum relating to the first mode (the lowest frequency maximum) was found. The convergence data is shown in figure 15.

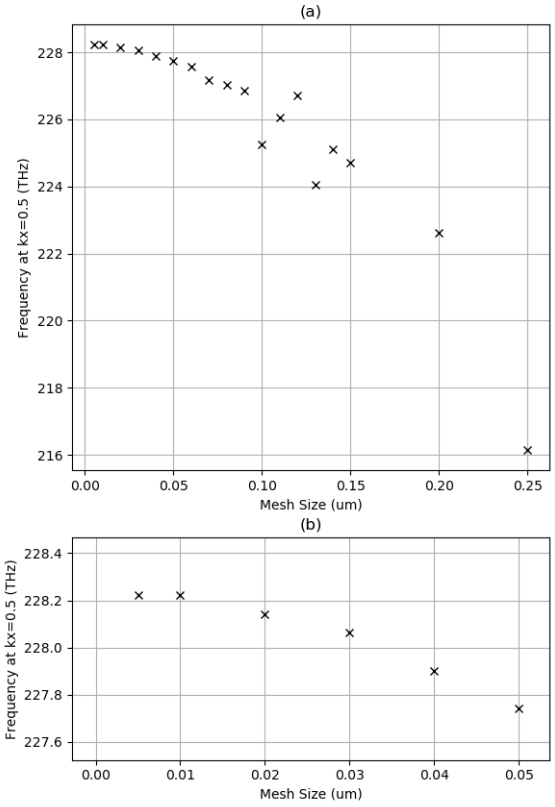

Figure 15: Figure (a) shows the frequency given by the time monitor method converging as the FDTD mesh size is decreased. Figure (b) shows a close up view of the most accurate 6 mesh sizes tested. Mesh sizes between 0.005μm and 0.01μm gave the same frequency of 228.223THz.

Figure 15 shows that the time monitor method does converge with FDTD simulation accuracy. However, it was found that all mesh sizes below 0.01μm gave the same value of frequency. This suggests that Lumerical is restricting the mesh size used to a minimum of 0.01μm explaining why all mesh sizes below this minimum do not give a more accurate frequency. Another explanation is that the frequency value is converged to the point that changing the mesh size results in negligible changes in frequency, however looking at the convergence of larger mesh sizes in figure 15(b) it does not seem likely that the frequency was within negligible error of the "true" value. It was concluded that the method was adequately converged at a mesh accuracy of 0.01μm for the method to be useful.

Before comparing the modes found by the time monitor method to those found by the mode monitor method, the validity of the mode monitor method can be tested through convergence testing too. The mode monitor was run for one specific frequency at a range of different mesh sizes and the output value of effective refractive index for the first mode was recorded. These were run on the same positive index waveguide as used previously and the converged frequency found at k_x by the time monitor convergence test was used. Using equation 10 the values of effective refractive index have been converted to the x-component of the wavenumber, k_x. The converted data is shown in figure 16 and it can be clearly seen that the method converges as mesh accuracy is increased, improving confidence in the mode monitor method at small mesh sizes. Using mesh sizes lesser than 0.06μm gave normalised k_x values within 2×10^{-4} of each other and the method was considered adequately converged.

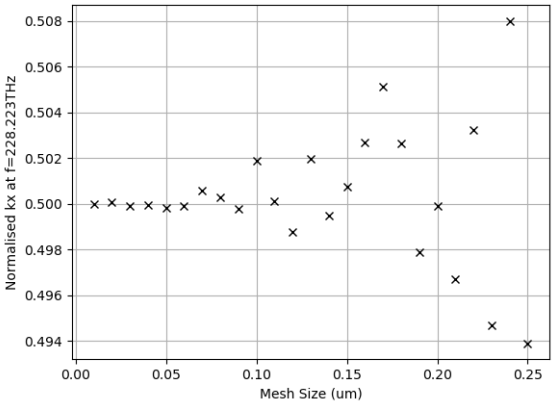

Figure 16: A graph of the normalised x-component of wavenumber found for the first mode by the mode monitor method at a frequency of f=228.223THz.

Finally, the two methods were compared by using each to find the fundamental transverse electric (TE) and transverse magnetic (TM) modes in the positive index waveguide. The mode monitor method automatically excites all possible polarisations and outputs them as different modes. This method was used and the values of effective frequency were converted to values of k_x. The orientation of the dipoles in the time monitor method were positioned once to produce TE modes and once to produce TM modes. Mesh sizes of 0.01μm were used and the default runtime of 1000fs was used for the time monitor method. The continuous data from the time monitor method, which contained the maxima related to the dispersion relations, were run through a python program to find the maxima and plot them as discrete points. The dispersion relation data was then "unfolded" (as explained in section 1.3) to span k_x values from 0 to 1. The data from both methods were plotted for comparison in figure 17.

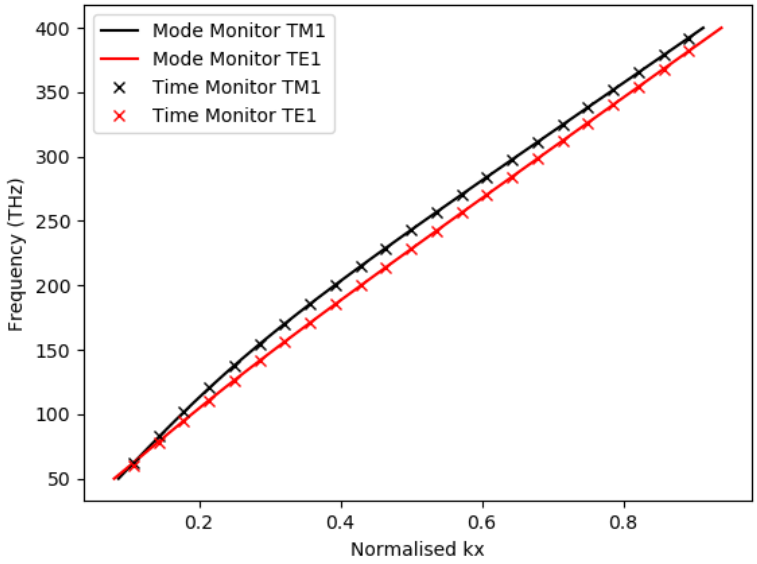

Figure 17: A graph showing the dispersion relations for the fundamental TE and TM modes calculated by the mode monitor method (solid line) and the time monitor method (crosses).

As shown in figure 17, the two methods for calculating the dispersion agree almost perfectly on the dispersion relations of the two fundamental modes. This increases confidence in the accuracy of the time monitor method.

4.3 Finding the Modes

In an attempt to find and characterise modes in a negative index waveguide the time monitor method was applied to a waveguide made of the same material created in section 2 using equations 7 and 8. Due to the dispersive nature of equations 7 and 8, negative index was only expected to be found at a specific range of wavelengths. Figure 18 shows how the real part of the refractive index changes with frequency and how each refractive index value relates to the dispersion relation. It was found that using an FDTD simulation runtime of 3000fs resulted in sufficient resolution of modes at the refractive indices of interest. Once again, increasing the runtime created an artefact around normalised k_x values of 0.1 but it was concluded that the increased resolution outweighed the obscuring of some of the frequency data at specific k_x values.

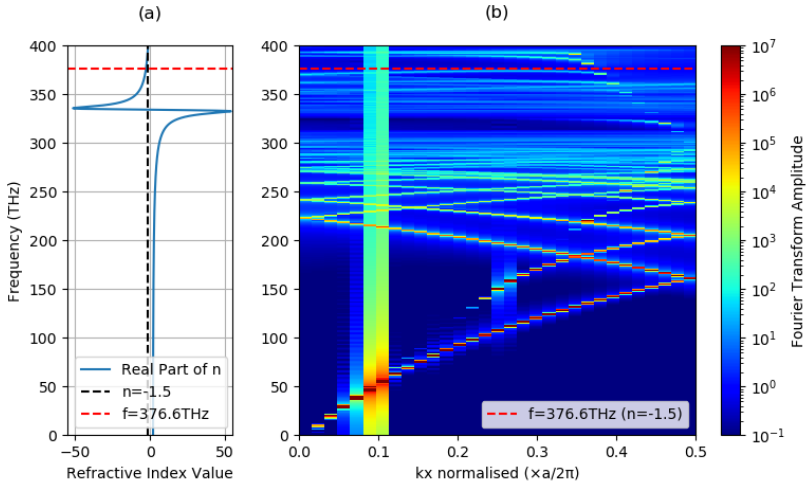

Figure 18: Figure (a) shows how the real part of refractive index changes with frequency. Figure (b) shows the dispersion relation for a waveguide with the material shown in figure (a). Lines showing where the refractive index is -1.5 are overlaid on the two plots.

As expected from figure 18(a), for the lower frequencies where the refractive index is positive, the modes in figure 18(b) look similar to those found in the positive index waveguide in figure 17. However, at higher frequencies, where the refractive index becomes negative, the modes' shapes change. Figure 19 shows a close up of the same figures at the negative index frequencies as well as some of the positive index frequencies.

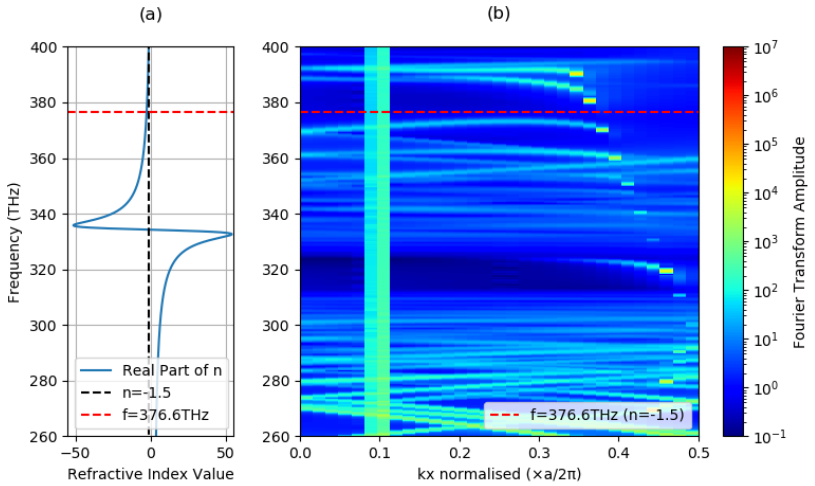

Figure 19: A close-up of figure 18 showing the negative index frequencies as well as some of the positive index frequencies.

4.4 Analysis and Discussion of Group Velocity in Negative Index Modes

Figure 19 shows two modes with turning points between frequencies 360 and 380THz, close to where the refractive index reaches -1.5. These turning points do not occur in positive index waveguides [3] and agree with the finding in T Lawrie's 2018 dissertation that a negative index waveguide provides modes which have turning points [3]. The turning points imply that some frequencies can excite multiple modes of the same order i.e. there are ranges of frequencies at which a mode is doubly degenerate [3]. No turning points were observed at the frequencies at which the material had a positive index of refraction. This reduces the doubt that the turning points are a product of the FDTD method and increases confidence that they are a product of the waveguide having a negative index of refraction. As explained in section 1.3.4, with the use of equation 12, the gradient of the dispersion relation in frequency and wavenumber can be used to find the group velocity as a function of wavenumber. This was done for the two most prominent negative index modes exhibiting turning points between frequencies 360 and 380THz and is shown in figure 20. While the data has been "unfolded" where band folding has been observed, the resolution is not great enough to find the origin of the modes and therefore can not be unfolded fully. Therefore, it is likely that the values of normalised k_x shown in figure 20 are offset by an integer value of the normalised k_x denoted by "i" in the figure. This has no bearing on the group velocities calculated however, as they are calculated from the gradient of the dispersion relation. The frequency data was normalised too to give a group velocity that was normalised in units of 1/c.

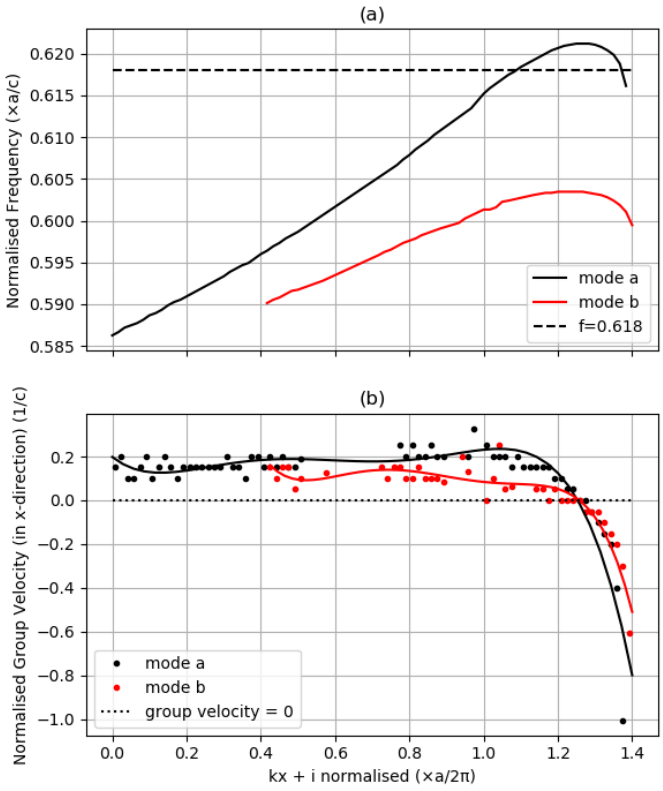

Figure 20: A graph of group velocity is shown in (b) by finding the gradient of the dispersion relations in (a). Arbitrary polynomials have been fit to the data in (b) in an attempt to smooth the data and make it easier to read. It is illustrated that a turning point in the dispersion relation equates to a group velocity of 0. The x-axis is offset by an unknown integer, "i".

It can be seen from figure 20b that the group velocity can reverse within modes. The modes seemed to cut-off as the group velocity approached -c, however the final point in "mode a" was found to have a normalised group velocity of -1.005. As seen at lower wavenumbers the data is noisy, the group velocities often vary by 0.05 normalised units (1/c) from the fit polynomial. It is therefore likely that this point below -1 is due to imperfect resolution in the time-monitor FDTD method used. Figure 20a shows how a mode can be doubly degenerate, at one frequency, as the dashed line at 371THz crosses "mode a" at two points. Provided these modes have only one turning point each, each pair of solutions at a specific, degenerate frequency will have group velocities of opposite sign, as

the group velocity is equivalent to the gradient of the dispersion relation. This means a single frequency can excite two guided modes, of the same order (same number of nodes and anti-nodes) which travel in opposite directions. Furthermore, at the turning points light will be transmitted with a group velocity of 0, rendering the mode stationary.

Other modes could be searched for by adjusting the values input into equations 7 and 8, giving negative permittivity and permeability at different frequencies and looking for negative index modes at those frequencies. One difficulty with adjusting the parameters of these equations is that to adjust the negative index frequency range, ω_e must be adjusted. Increasing ω_e results in a decrease in the frequencies at which negative index is found, however it also results in a decrease in the size of the frequency range at which the refractive index is negative, limiting the range of frequencies any negative refractive index modes can exist for. It was also found that making other parameters such as χ and $\Delta\varepsilon$ or $\Delta\mu$ negative to increase the range of negative index frequencies resulted in simulations diverging from true values.

5 Conclusions

5.1 Summary of Findings

This project investigated the viability of waveguides made of negative refractive index materials using the finite-difference time-domain numerical method. The loss in negative index materials was investigated. It was found that the absorptivity in negative index materials obey the Beer-Lambert law, which would be the limiting factor in the power of guided modes transmitted through a negative index waveguide.

Two modes were found and studied in a negative refractive index waveguide with the finite-difference time-domain method and their dispersion relations were plotted. It was found that some modes in negative index waveguides have turning points in their dispersion relations implying an inversion of group velocity within the same mode, as well as double degeneracy at certain frequencies within one mode (the same mode can be excited at two different wavenumbers by the same wavelength of light). Double degeneracy was found at frequencies between 370 and 372THz and 360 and 362THz for each mode respectively with turning points being found at the top of those frequency ranges. The group velocity was found to be between 0 and 0.2 (normalised 1/c units) for the majority of wavenumbers before approaching -1 at the highest wavenumbers. To the author's knowledge, this is the first time the finite-difference time-domain method has been used to find modes in negative refractive index waveguides and to confirm novel phenomena in negative refractive index waveguide modes. Both the double degeneracy and inverting group velocity findings are consistent with 2002 [1], 2003 [2] and 2018 [3] papers on the subject using other techniques. As mentioned in the 2003 paper [2] this diverse dispersion in group velocity could have useful applications in optical technologies such as optical data storage and quantum computing.

5.2 Further Investigation

It would be useful to find and characterise more modes in the negative index waveguide at different frequencies. As discussed in section 4.4, the material used in this project does not provide much freedom in the frequencies at which negative refractive index is found. A more versatile negative refractive index material could be developed in Lumerical in order to find and characterise more modes in a negative refractive index waveguide, testing whether the novel properties found in this project are true for all modes and to search for more novel properties. Furthermore if a method was found which allowed for the dispersion relations to be "unwrapped" fully, then exact wavenumber data could be found for the dispersion relations of the modes allowing for more analysis, such as the calculation of phase velocity.

Acknowledgments

I would like to thank my project supervisor, Dr Daryl Beggs, who helped teach me how to perform a scientific project, helped me understand the technicalities of this project and guided the project to an interesting conclusion.

References

[1]I. V. Shadrivov, A. A. Sukhorukov, and Y. S. Kivshar, "Guided modes in negative-refractive-index waveguides", Physical Review E **67**, 057602 (2003).

[2]A. Peacock and N. Broderick, "Guided modes in channel waveguides with a negative index of refraction", Optics Express **11**, 2502–2510 (2003).

[3]T. M. Lawrie, "Can waveguides function when constructed from negative refractive index materials? the theory of left-handed waveguide modes", School of Physics and Astronomy, Cardiff University, 29–33 (2018).

[4]V. G. Veselago, "Reviews of topical problems: the electrodynamics of substances with simultaneously negative values of epsilon and mu", Soviet Physics Uspekhi **10**, R04 (1968).

[5]L. Rayleigh, "Xxxi. investigations in optics, with special reference to the spectroscope", The London, Edinburgh, and Dublin Philosophical Magazine and Journal of Science **8**, 261–274 (1879).

[6]J. B. Pendry, "Negative refraction makes a perfect lens", Physical review letters **85**, 3966 (2000).

[7]D. R. Smith, W. J. Padilla, D. Vier, S. C. Nemat-Nasser, and S. Schultz, "Composite medium with simultaneously negative permeability and permittivity", Physical review letters **84**, 4184 (2000).

[8]R. Shelby, D. Smith, S. Nemat-Nasser, and S. Schultz, "Microwave transmission through a two-dimensional, isotropic, left-handed metamaterial", Applied Physics Letters **78**, 489–491 (2001).

[9]R. A. Shelby, D. R. Smith, and S. Schultz, "Experimental verification of a negative index of refraction", science **292**, 77–79 (2001).

[10]F. R. Connor, *Wave transmission* (London: Edward Arnold, 1972).

[11]D. M. Sullivan, *Electromagnetic simulation using the fdtd method* (John Wiley & Sons, 2013), pp. 53–54.

[12]Lumerical, "Convergence testing process for fdtd simulations", support.lumerical.com/hc/en-us/articles/360034915833-Convergence-testing-process-for-FDTD-simulations, Accessed 12/12/2019.

[13]Lumerical, "Bulk metamaterials", apps.lumerical.com/metamaterials_bulk_metamaterials.html, Accessed 9/12/2019.

[14]D. Swinehart, "The beer-lambert law", Journal of chemical education **39**, 333 (1962).

[15]G. B. Whitham, *Linear and nonlinear waves*, Vol. 42 (John Wiley & Sons, 2011), pp. 364–365.

[16]M. Hayes and M. Musgrave, "On energy flux and group velocity", Wave motion **1**, 75–82 (1979).

[17]Wikimedia, "1d empty lattice approximation", commons.wikimedia.org/wiki/File:1D-Empty-Lattice-Approximation.svg, Accessed 3/5/2020.

[18]G. Woan, *The cambridge handbook of physics formulas* (Cambridge University Press, 2000).

[19]Lumerical, "Mode expansion monitor - simulation object", support.lumerical.com/hc/en-us/articles/360034902413-Mode-expansion-monitor-Simulation-object, Accessed 29/4/2020.